AN ANALYTICAL APPROACH TO DERIVE CONSTITUTIVE LAWS FROM BENDING TESTS WITHOUT USING FE-SIMULATION

Philipp Hadl (1) and Nguyen-Viet Tue (1)

(1) Institute of Structural Concrete, Graz University of Technology, Austria

Abstract

This paper presents an analytical approach to derive constitutive laws from force or flexural tensile stress - mid-span deflection relationships obtained in 4-point-bending tests. The load bearing behaviour in bending is divided into hardening and softening phase. It is assumed that the section remains plane until the peak-load is reached in the bending test. Initially, the curvature at peak load is determined with the mid-span deflection and force at load maximum from the experiment. Therefore the principle of virtual work by double integration of the curvatures along the length of the prism is used. Consequently, the stress-strain relationship until peak-load is determined directly by using two assumptions for stress development in this area. In the softening phase the cross-section does not remain plane. By assuming a characteristic length, the stress-strain response for the softening branch is defined. Finally, the derived constitutive laws are compared with finite element simulation and other numerical and analytical approaches. All calculations verify the accuracy of the model.

Résumé

Cet article présente une approche analytique afin d’obtenir les lois de comportement à partir de courbes force ou contrainte équivalente en flexion - flèche à mi-portée obtenues lors d’essais de flexion 4 points. Le comportement sous charge en flexion est divisé entre une phase écrouissante et une phase adoucissante. On suppose que la section reste plane jusqu’à ce que la charge maximale soit atteinte dans l’essai de flexion. Initialement la courbure au pic d’effort est déterminée à partir de la flèche et de la contrainte à mi-portée sous la charge maximale obtenue dans l’expérience. On utilise pour cela le principe des travaux virtuels par double intégration des courbures le long du prisme. En conséquence la relation contrainte-déformation jusqu’au pic d’effort est déterminée directement en utilisant deux hypothèses pour la distribution des contraintes dans cette zone. Dans la phase adoucissante la section droite ne reste pas plane. En postulant une longueur caractéristique, la relation contrainte-déformation peut être établie pour la branche adoucissante. Finalement, les lois de comportement obtenues sont comparées avec un calcul aux éléments finis et d’autres approches numériques et analytiques. Tous les calculs vérifient la précision du modèle.

1. INTRODUCTION

The tensile stress-strain response of ultra-high-performance fibre-reinforced concrete (UHPFRC) is a fundamental constitutive property, and reliable knowledge of this response is necessary for the design of tensile-carrying elements. Flexural test methods, whose implementation is well-established, present a test procedure capable of assessing this property. Nevertheless, these methods provide indirect information and need to be complemented by inverse analysis to quantify the intrinsic tensile behaviour of tested materials [1].

Analytical inverse analyses for four-point flexural tests on UHPFRC or high-performance fibre-reinforced cementitious composites (HPFRCCs) have been developed by many researchers, such as [1] - [10], which are summarized and explained in [1], [2] and [3]. Baby et al. [3] define flexural test methods for strain-hardening and strain-softening behaviour depending on the expected crack distance in the bending test. For expected strain-hardening behaviour they differentiate between methods based on strain measurement on the specimen's tensile face (such as [1] or [5]) and methods based on deflection measurement (such as [2], [8] or [9]). In case of strain-softening behaviour analysing methods based on crack-opening measurements or deflection measurements have been defined by [11].

In case of strain-hardening material and test set-up with deflection measurement, the approaches proposed by [2], [8], [9] or [10] convert the "bending moment versus mid-span deflection experimental response" into a "bending moment – curvature response". For this purpose different assumptions about the shape of the curvature along the specimen are used in the mentioned articles. In [2], an iterative displacement to curvature transformation is proposed based on the double integration of the curvature along the length of the prism. Consequently the stress-strain relationship is determined by point-by-point inverse analysis similar to the approach in [9]. Nevertheless, this method requires post-processing [10]. In addition, a simplified approach by using a bilinear stress-strain relationship is proposed in [2] and [5], which is assumed to be convenient for design or FEM analysis by the authors.

However, many authors, such as [1] [2] or [12] define constitutive laws only for the loading branch until the peak-load is reached in the bending test. In contrast, approaches to characterize the unloading branch (crack-opening; fibre pull-out) are made in [6], [10] and [13] for instance. The French AFGC guidelines ([5]) assume the tensile stress to be zero at crack width $l_f/4$ for reasons of simplification.

The main aim of this research is to develop a new inverse analysis methodology without using FEM, which is easy to implement, reliable, quick and mechanically consistent. The presented model is valid for strain-hardening as well as strain-softening behaviour and describes both the loading and the unloading branch of the constitutive law.

2. MODEL DESCRIPTION

The analytical model derives constitutive laws (stress-strain relationships) from force or flexural tensile strength - mid-span defection relationships obtained in 4-point-bending tests. It can be used for normal strength concrete as well as UHPC and has been developed primarily for beams with deflection-hardening behaviour, but it is also applicable for beams with deflection-softening behaviour. Since UHPC has to fulfil a non-brittleness criterion [5], UHPFRC usually shows deflection-hardening behaviour for structural applications. In special cases, such as high loaded columns, the required ductility can be guaranteed by confinement with conventional reinforcement, see [14] for instance. However, the presented investigations focus on deflection-hardening behaviour.

The stress-strain relationship presented in Figure 1 is defined as basis for the analytical model, as proposed in [15]. Thereby, the constitutive-law is divided into three phases. Phase I represents the quasi-linear-elastic behaviour until the tensile matrix strength $f_{ct,0}$ is reached (loss of linearity; point 1 in Figure 1). Phase II describes the hardening behaviour until the residual tensile strength $f_{ct,r}$ is reached, which is equal to the peak-load in the bending test (point 2 in Figure 1). The softening phase (III) starts after the peak load has been exceeded and until the pre-defined maximum tensile strain $\varepsilon_{ct,r2}$ is reached (point 3 in Figure 1). It is characterized by fibre pull-out in the localized crack and unloading.

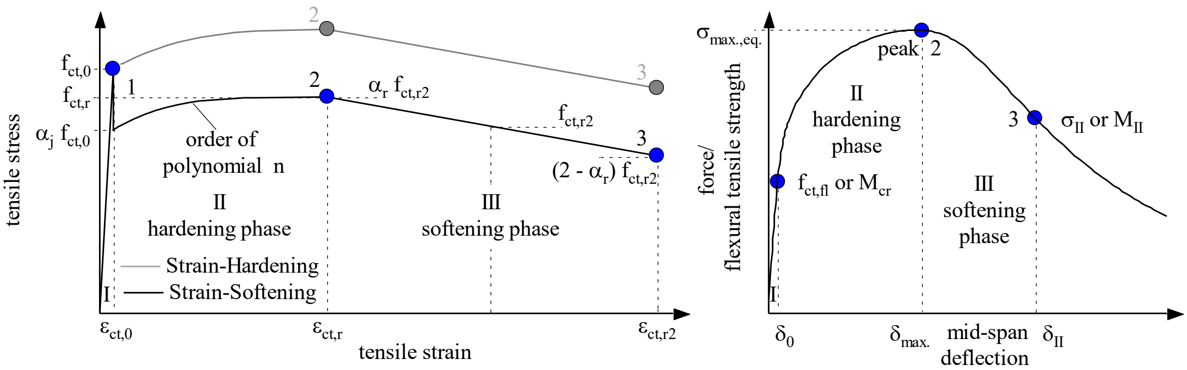

Figure 1: Basic scheme of the stress-strain relationship in the analytical model (left) and associated phases in the 4-point-bending test

In phase I the tensile matrix strength $f_{ct,0}$ and the associated strain $\varepsilon_{ct,0} = f_{ct,0}/E_{cm}$ are significant. In phase II, the following parameters are defined:

- factor α_j to consider the drop after exceeding the tensile matrix strength $f_{ct,0}$ ($\alpha_j < 1$ for strain-softening; $\alpha_j = 1$ for strain-hardening)
- residual tensile strength $f_{ct,r}$ and associated strain $\varepsilon_{ct,r}$
- order of polynomial n to describe the stress development between $f_{ct,0}$ and $f_{ct,r}$
- flexural tensile strength at peak-load $\sigma_{max.,eq.}=M/W$
- mid-span deflection at peak-load $\delta_{max.}$

In phase III the following parameters are essential:

- bending moment M_{II} and associated deflection δ_{II} when reaching the maximum tensile strain $\varepsilon_{ct,r2}$
- residual tensile strength $f_{ct,r2}$ due to M_{II}
- factor α_r to describe the slope of the stress-strain relationship during crack localization

The maximum tensile strain $\varepsilon_{ct,r2}$ defines the end of the design-relevant area of the constitutive law. Since the approaches for $\varepsilon_{ct,r2}$ differ in a wide range depending on the guideline, values of 15, 20 or 25‰ can be selected in the model.

2.1 Input parameters

The required input parameters are demonstrated in Table 1. In addition to material input parameters the definition of the beam geometry is necessary. Further, input of the flexural tensile strength - mid-span deflection relationship obtained in experiment is required.

Table 1: Input parameters

tensile matrix strength $f_{ct,0}$	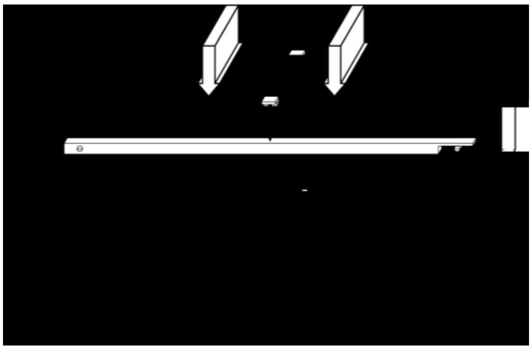
elastic modulus of UHPC E_{cm}	
fibre length l_f	
factor α_j	
order of the parabola n	
maximum tensile strain $\varepsilon_{ct,r2}$	
factor α_r	
mid-span deflection at peak-load $\delta_{max.}$	
flexural tensile strength at peak-load $\sigma_{max.,eq.}=M/W$	area of bending moment M_{II} and deflection δ_{II}

2.2 Hardening phase – multiple-cracking

Phases I and II are summarized in the model description. As mentioned, phase I ends with the loss of linearity. In phase II, multiple cracks are formed, until the peak-load is reached and the localization in the weakest crack occurs in phase III. In case of deflection-softening behaviour, phase II is skipped. Consequently localization and crack-opening starts immediately after the first crack. A detailed description of the load-deformation behaviour of fibre reinforced bending beams is presented in [15] and [16] for instance.

In order to consider the size effect, the direct tensile matrix strength $f_{ct,0}$ is converted into flexural matrix strength $f_{ct,fl}$ (nonlinear behaviour initiation point; see Figure 1). Therefore the approach of [4] and [17] according to equation 1 is used. The associated deflection δ_0 is calculated by assuming linear-elastic behaviour.

$$f_{ct,fl} = \frac{f_{ct,0}}{\dfrac{2 \cdot (h/h_0)^{0.7}}{1 + 2 \cdot (h/h_0)^{0.7}}} \tag{1}$$

Further, the coefficient $\alpha_{j,fl}$ is defined from the factor α_j to consider the size effect:

$$\alpha_{j,fl} = \alpha_j \cdot \frac{f_{ct,0}}{f_{ct,fl}} \tag{2}$$

In principle, the mid-span deflection δ is calculated with the principle of virtual work by integrating the curvature and the virtual moment along the beam (double integration of curvature; equation 3). Therefore, the definition $\varkappa$=M/EI is used and the curvature remains constant in the zone of constant bending moment. Note, that this approach is only valid if the crack spacing in the experiment s_r is smaller than l_f. The static and virtual system as well as the curvature for 4-point-bending tests with load application at the third points is demonstrated in Figure 2. Similar approaches have been used in [2] [8], [9] or [10] for instance.

$$\delta = \frac{1}{EI}\cdot\int_0^l \overline{M_{(x)}}\cdot M_{(x)}\, d_x = \int_0^l \overline{M_{(x)}}\cdot \varkappa_{(x)}\, d_x \tag{3}$$

The curvature at peak-load $\varkappa_P$ is determined by equation 4, which results from transforming equation 3, according to [15] ($\delta = \delta_{max.}$; $M_P = \sigma_{max.,eq.}\cdot W$; see input parameters). The exponent k considers the nonlinear curvature distribution between the curvature at crack moment $\varkappa_{cr}$ and $\varkappa_P$. A value of 0.6 is recommended in [15] and used in this investigation.

$$\varkappa_P = \frac{\frac{27\delta}{l_{ef}^2} - \frac{2f_{ct,fl}}{E_{cm}h}\left(\left(\frac{M_{cr}}{M_P}\right)^2 + \frac{1}{2}\left(\frac{M_{cr}}{M_P}\right)^k + \frac{1}{2}\left(\frac{M_{cr}}{M_P}\right)^{k+1} - \left(\frac{M_{cr}}{M_P}\right)^{k+2}\right)}{\left(\frac{M_{cr}}{M_P}\right)^k - \frac{1}{2}\left(\frac{M_{cr}}{M_P}\right)^{k+1} - \frac{1}{2}\left(\frac{M_{cr}}{M_P}\right)^{k+2} + \frac{15}{8}} \tag{4}$$

Figure 2: Determination of the curvature at peak-load according to [15]

Linear strain distribution over the cross-section height is assumed until the peak-load is reached in bending test, which means the section remains plane between $f_{ct,0}$ and $f_{ct,r}$. The results of FE-simulations verify this assumption, as described in [18]. Linear-elastic material behaviour is used to calculate the compressive force F_c and the tensile matrix force $F_{ct,0}$.

Consequently, the residual tensile strength $f_{ct,r}$ and the associated strain $\varepsilon_{ct,r}$ are determined directly by equilibrium in the cross-section. Since the curvature at peak-load $\varkappa_P$, the external bending moment $M_P = \sigma_{max.,eq.}\ W$ and the tensile matrix strength $f_{ct,0}$ are known, $f_{ct,r}$ is calculated based on equilibrium of the horizontal forces and bending moments [15]. As mentioned above, the values for $\alpha_{j,fl}$ and the order of the parabola n have to be defined in advance. Consequently, the compressive zone height x, $\varepsilon_{ct,r}$ and $f_{ct,r}$ are known. Figure 3 shows the stresses and strains in the section. More information has been published in [18].

Additional points between the first crack (point 1 in Figure 1) and peak-load (point 2 in Figure 1) are calculated by varying the curvature $\varkappa_{cr} \leq \varkappa_i \leq \varkappa_P$. Since the cross-section remains plane and the constitutive law is known, the associated strain and deflection are determined by equilibrium of horizontal forces and bending moments.

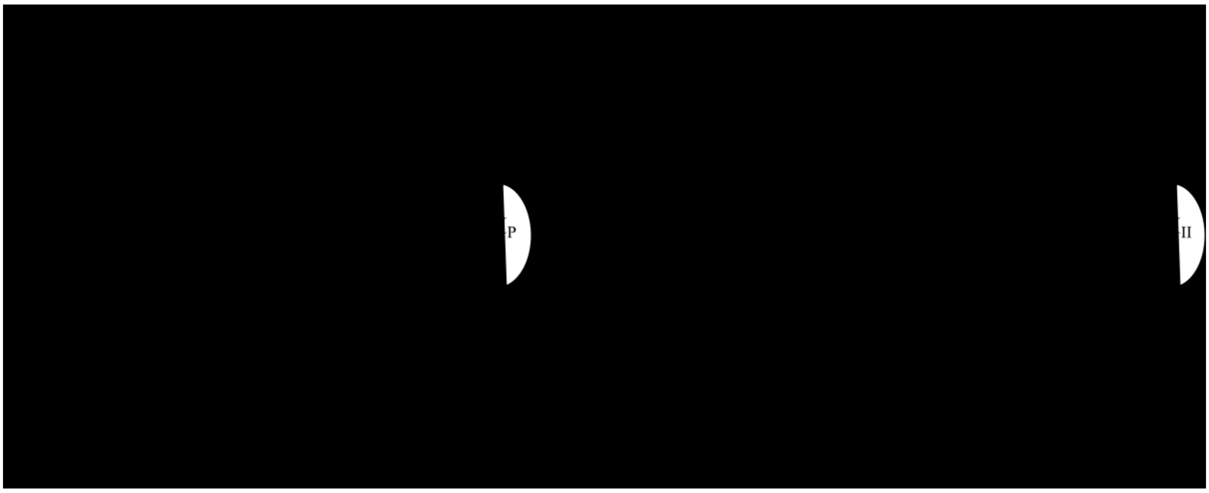

Figure 3: Strains, stresses and crack widths to define $f_{ct,r}$ (left) and $f_{ct,r2}$ (right)

By comparing the determined flexural tensile strength - mid-span defection relationship with experimental results, the values for α_j and n are verified and adapted if required. This is an iterative process until sufficient correlation with the test results is given. Figure 4 shows schematically the determined stress-strain relationship as well as the flexural tensile strength - mid-span defection relationship until peak-load is reached.

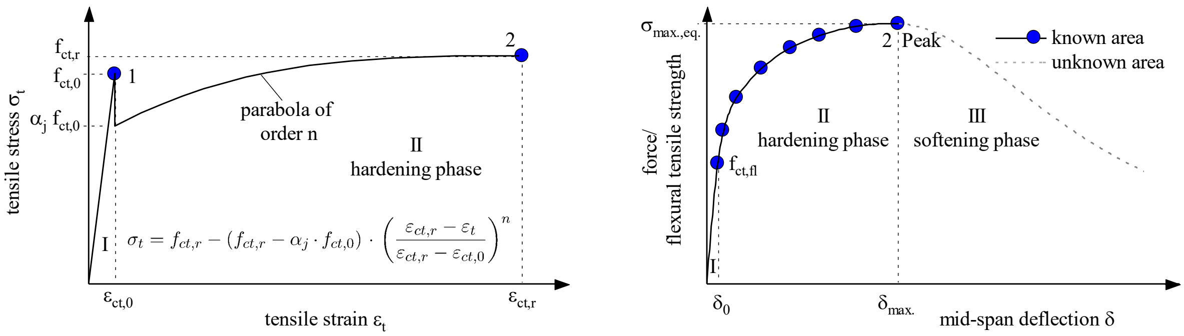

Figure 4: Determined stress-strain relationship (left) and flexural tensile strength - mid-span defection relationship for phases I + II (right)

2.3 Softening phase – crack-opening

The softening phase (phase III in Figure 1) starts after the peak-load has been reached in bending test. It is characterized by failure crack localization and fibre pull-out, while the rest of the specimen is unloaded. The constitutive law in the unloading branch is linear until $\varepsilon_{ct,r2}$ is reached, as can be seen in Figure 1. Its slope in this area is characterized by the factor α_r.

Due to the crack opening, the deflection is concentrated in the macro-crack and the cross-section does not remain plane. Consequently there is no tensile strain, but a crack opening w_{cr} of the macro-crack. According to [19], the crack width is converted to tensile strain by assuming a characteristic length. The characteristic length l_{local} has been investigated in [18] and [20] in detail. Consequently, the results of [20] are used in this investigation, where l_{local} is estimated depending on $\varepsilon_{ct,r2}$, bending slenderness l_{ef}/h, curvature at peak-load $\varkappa_P$ and beam height h. Linear interpolation should be performed between the individual values.

$$l_{local} = \frac{2}{3} \cdot h - \frac{h + (25 - \varepsilon_{ct,r2}) \cdot 7.5}{600} \cdot \varkappa_P \qquad \text{for } l_{ef}/h = 4 \tag{5}$$

$$l_{local} = \left(h + \left(\varepsilon_{ct,r2} - 15\right)\right) - \frac{3}{20} \cdot \varkappa_P \qquad \text{for } l_{ef}/h = 12$$

Initially, the definition of point 3 in Figure 1 is required, where $\varepsilon_{ct,r2}$ is reached in the flexural tensile strength - mid-span defection relationship of the experiment. It is defined by the bending moment M_{II} and the associated deflection δ_{II}. Therefore the crack width $w_{local,requ}$ due to opening of the failing crack excluding the crack width at peak load is determined:

$$w_{local,requ.} = l_{local} \cdot \left(\varepsilon_{ct,r2} - \varepsilon_{ct,r}\right) \tag{6}$$

Subsequently, an arbitrary point in the unloading branch is selected where $\varepsilon_{ct,r2}$ should be reached in the experiment (moment $M_{II,i}$ and deflection $\delta_{II,i}$). The deflection $\delta_{LOK,i}$ which results from crack-opening theoretically, is calculated by $\delta_{II,i}$ deducing deflection beyond localization $\delta_{OL,i}$ for considering reversible deformation components. Reversible deformation components occur, since the force in the bending test decreases (unloading), and thus the curvature and deflection in the area beyond the localization reduce. The approach to consider reversible deformations has been described in [18] as well as [20] and has been verified by experimental investigations in [18]. In this approach 50 percent of the curvatures beyond the localization area, are reversible if the specimen is totally unloaded. Figure 5 shows the procedure to determine $\delta_{LOK,i}$ schematically.

$$\delta_{II,i} = \delta_{OL,i} + \delta_{LOK,i} \qquad \Rightarrow \delta_{LOK,i} = \delta_{II,i} - \delta_{OL,i} \tag{7}$$

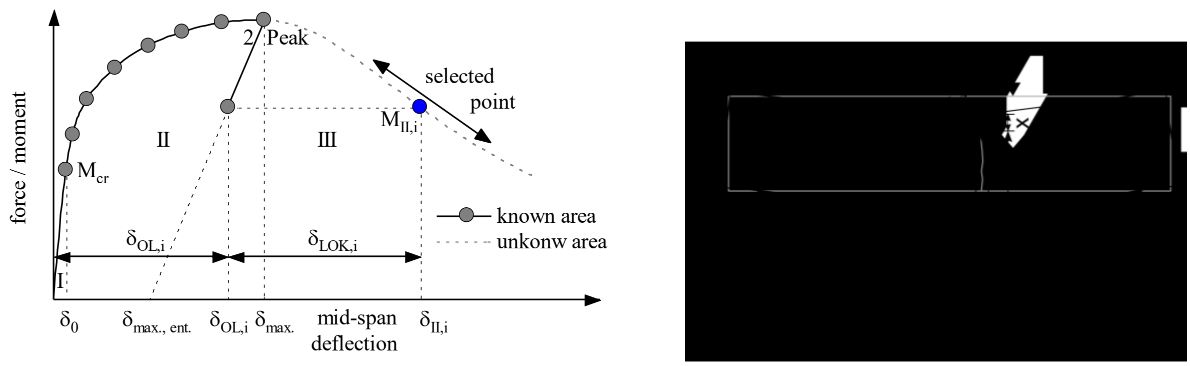

Figure 5: Determination of $\delta_{LOK,i}$ (left) and rigid block movement to determine $w_{local,calc.}$

In order to determine the calculated crack width $w_{local,calc}$ caused by $\delta_{LOK,i}$, the crack-opening is considered as hinge between two perfectly rigid blocks as can be seen in Figure 5.

$$w_{local,calc.} = \frac{\delta_{LOK,i} \cdot \left(h - x_{II,i}\right)}{l_{ef} + x_r} + \frac{\delta_{LOK,i} \cdot \left(h - x_{II,i}\right)}{l_{ef} - x_r} \tag{8}$$

The required compressive zone height $x_{II,i}$ is estimated depending on $\varepsilon_{ct,r2}$, l_{ef}/h, $\varkappa_P$ h according to [18]. Linear interpolation should be performed between the individual values.

$$x_{II,i} = 10 - \frac{\varepsilon_{ct,r2} - 15}{2} + 0.1 \cdot \varkappa_P \qquad \text{for } l_{ef}/h = 4 \tag{9}$$

$$x_{II,i} = 3.4 - \frac{3}{25} \cdot \left(\varepsilon_{ct,r2} - 15\right) + 0.012 \cdot \varkappa_P \qquad \text{for } l_{ef}/h = 12$$

The point $M_{II,i}/\delta_{II,i}$ is iterated until the calculated crack width $w_{local,calc}$ is equal to the real crack width $w_{local,requ}$. The point M_{II}/δ_{II} at $\varepsilon_{ct,r2}$ is obtained when $w_{local,requ}=w_{local,calc}$. Alternatively, δ_{II} can be estimated according to [15] by equation 10 for reasons of simplification. The investigations in [18] verify the accuracy of the presented approach, while equation 10 is only valid for standardized beam specimens according to [21].

$$\delta_{II} = \frac{1}{1.2} \cdot l_{local} \cdot \left(\varepsilon_{ct,r2} - \varepsilon_{ct,r}\right) + \delta_{max}. \tag{10}$$

Consequently, the compressive zone curvature $\varkappa_{II}$ of point M_{II}/δ_{II} is determined, by the principle of virtual work (double integration of curvature). Figure 6 demonstrates the static system, the curvature and the virtual system. The curvature $\varkappa_{II}$ results from converting equation 3. For further information, see [18].

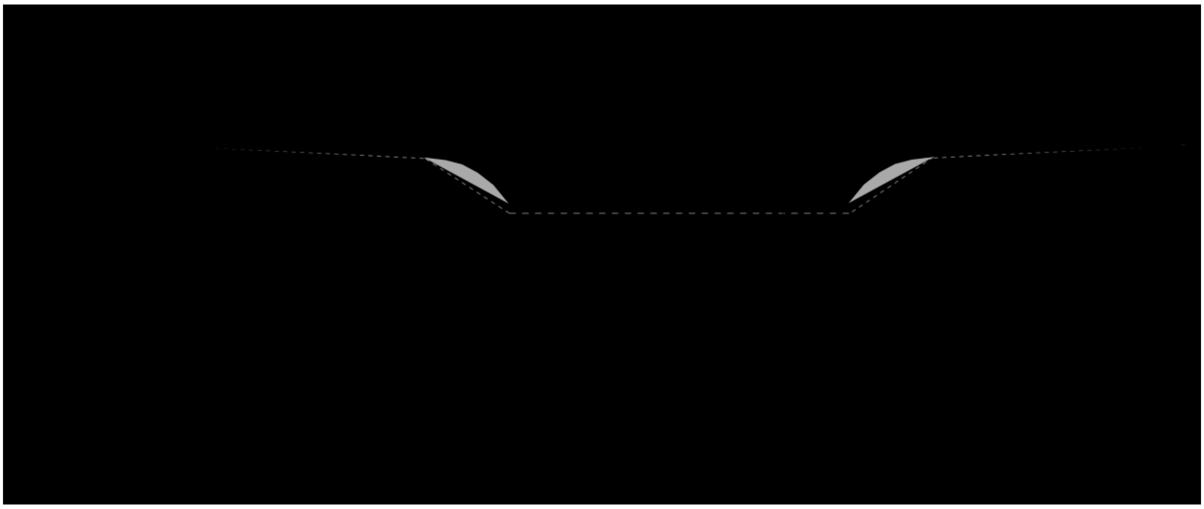

Figure 6: Static system, curvature and virtual system in phase III (unloading branch)

Since the curvature $\varkappa_{II}$, the external bending moment M_{II} and the constitutive law until peak-load are known, the residual tensile strength $f_{ct,r2}$ is determined directly based on equilibrium in the cross-section (equilibrium of horizontal forces and bending moments). As mentioned above the value for α_r has to be defined in advance.

It is significant, that the cross-section in this area does not remain plane. Therefore, the cracked tension zone is described by crack-opening according to equation 11. Linear crack path over the cross-section height is assumed. Figure 3 shows the stresses, strains and crack widths in the section. To determine the compressive force F_c and the tensile matrix force $F_{ct,0}$ a linear-elastic material behaviour is used still. The results in [18] verify this assumption.

$$w_{bottom} = w_P + l_{local} \cdot \left(\varepsilon_{ct,r2} - \varepsilon_{ct,r}\right) = l_f \cdot \varepsilon_{ct,r} + l_{local} \cdot \left(\varepsilon_{ct,r2} - \varepsilon_{ct,r}\right) \tag{11}$$

The tensile strength $f_{ct,r2u}$ at maximum tensile strain $\varepsilon_{ct,r2}$ is determined by $f_{ct,r2u} = (2 - \alpha_r) \cdot f_{ct,r2}$. Figure 7 shows the calculated stress-strain and flexural tensile strength - mid-span defection relationship. The factor α_r has to be defined in a way that $\alpha_r \cdot f_{ct,r2}$ is equal to $f_{ct,r}$. Since the constitutive law between $\varepsilon_{ct,r}$ and $\varepsilon_{ct,r2}$ is linear, the flexural tensile strength - mid-span defection relationship between peak-load and M_{II} is also linear.

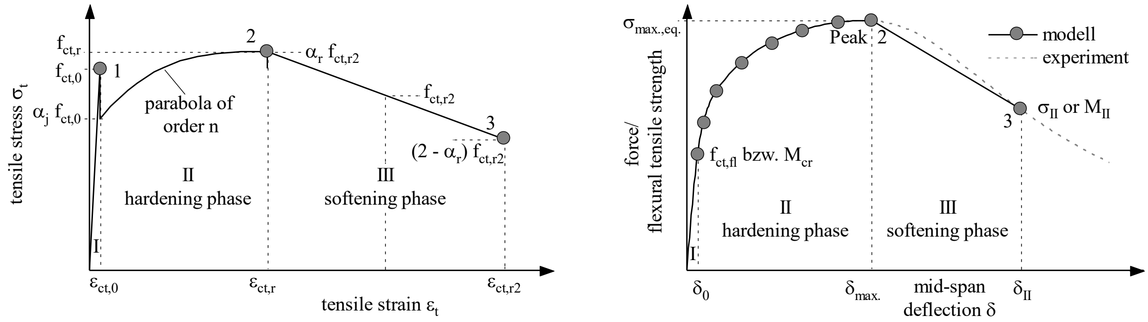

Figure 7: Determined constitutive law (left) and flexural tensile strength - mid-span defection relationship (right)

3. CALCULATION RESULTS

In [18] and [22] extensive experimental investigations on the bending behaviour of fibre reinforced UHPFRC have been conducted. The test program included 4-point-bending tests on standardized beams according to the German guideline for fibre concrete [21] (h = 150 mm) and on thin plates (h = 150 mm). Constitutive laws have been derived from the experimental response in the form of flexural tensile strength - mid-span defection relationships. The used input parameters have been published in [18].

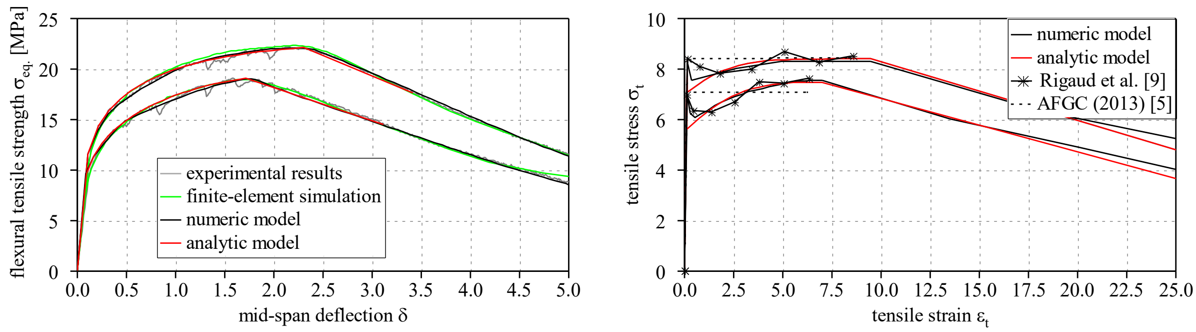

Figure 8: Calculated bending response (left) and derived constitutive laws (right)

The re-calculation of the experiments shows excellent correlation both in the area of multiple-cracking (phase I + II) and crack opening (phase III). Two representative tests (standardized beams) are depicted in Figure 8. Further, the results are compared with the numerical model presented in [20] and with finite element analysis. The analytical and numerical models as well as the FE-simulation give identical results. Consequently, the analytical model has been verified. In addition, the derived stress-strain relationships determined by the presented analytical and numerical model [20] can be seen in Figure 8. Further, the stress-strain relationships calculated according to the by point-by-point inverse analysis of Rigaud et al. [9] and the results of the simplified approach of AFGC [5] (Annex 4; chapter 3.2) are depicted. It is obvious that all approaches show sufficient correlation.

4. CONCLUSION

This paper presents an analytical approach to derive constitutive laws from force or flexural tensile strength - mid-span defection relationships obtained in 4-point-bending tests.

The load bearing behaviour in bending is divided in hardening phase until peak-load is reached and softening branch (crack-opening or fibre pull-out phase). Further, the accuracy of the model has been verified by comparison with results from a numerical model as well as finite element simulation and other analytical approaches. All methods give identical results.

REFERENCES

[1] Baby, F., Graybeal, B., Marchand, P. and Toutlemonde, F., 'Proposed Flexural Test Method and Associated Inverse Analysis for Ultra-High-Performance Fiber-Reinforced Concrete', *ACI Materials Journal.* **109** (2012) 545-556.
[2] Baby, F., Graybeal, B., Marchand, P. and Toutlemonde, F., 'UHPFRC tensile behaviour characterization: inverse analysis of four-point bending test results', *Mat. and Struct.* **46** (2013) 1337-1354.
[3] Baby, F., Graybeal, B., Marchand, P. and Toutlemonde, F., 'Identification of UHPFRC tensile behaviour: Methodology based on bending tests', in 'UHPFRC 2013', RILEM PRO 87, 649-658.
[4] AFGC, 'Ultra High Performance Fibre-Reinforced Concrete. Interim Recommend.', (Setra, 2002).
[5] AFGC, 'Ultra High Performance Fibre-Reinforced Concrete. Recommendations', (AFGC, 2013).
[6] Ostergaard, L., Walter, R. and Olesen, J., 'Method for Determination of Tensile Properties of Engineered Cementitious Composites', in 'Proceedings of ConMat'05', Vancouver, 2005.
[7] Kanakubo, T., 'Tensile Characteristics Evaluation Method for DFRCC', *Journal of Advanced Concrete Technology.* **4** (2006) 3-17.
[8] Qian, S. and Li, V., 'Simplified Inverse Method for Determining the Tensile Properties of SHCCs', *Journal of Advanced Concrete Technology.* **6** (2008) 353-363.
[9] Rigaud, S., Chanvillard, G. and Chen, J., 'Characterization of Bending and Tensile Behaviors of UHPCCGF', in 'Proceedings of HPFRCC 6', Ann Arbor, 2011.
[10] Lopez, J., Serna, P., Navarro-Gregor, J. and Camacho, E., 'An inverse analysis method based on deflection to curvature transformation to determine the tensile properties of UHPFRC', *Materials and Structures.* **48** (2015) 3703-3718.
[11] Baby, F., 'Contribution to Identification of UHPFRC Tensile Constitutive Behavior and Accounting for Structural Design', *PhD-Thesis.* (2012) Paris-Est University.
[12] Tailhan, J., Rossi, P. and Parant, E., 'Inverse numerical approach to determine the uniaxial tensile behaviour of a stress hardening cement composite from its bending behaviour', in 'Proceedings of BEFIB 2004', Varenna, 2004.
[13] Sorankom, C. and Mobasher, B., 'Closed-form moment-curvature expressions for Homogenized Fiber-Reinforced Concrete', *ACI Materials Journal.* **104** (2007) 351-359.
[14] Hadl, P., Vojvodic, G., Kim, H. and Tue, N.-V., 'Substitution of steel components by UHPC', in 'Proceedings of SEMC 2016', Cape Town, 2016.
[15] Gröger, J., 'Ein Beitrag zur Beschreibung des Zugtragverhaltens von stahlfaserverstärktem Beton', *PhD-Thesis in preparation.* (2017) HTWK Leipzig.
[16] Spasojewic, A., 'Structural Implications of UHPFRC in Bridge Design', *PhD-Thesis.* (2008) EPFL
[17] Fehling, E., Schmidt, M., Walraven, J., Leutbecher, T. and Fröhlich, S., 'Ultrahochfester Beton', in 'Betonkalender', 2013 (Ernst & Sohn, Berlin, 2013).
[18] Hadl, P., 'Zum besseren Verständnis der Streuung des Zugtragverhaltens von stahlfaserbewehrtem Normalbeton und Ultra-Hochleistungsbeton', *PhD-Thesis.* (2017) TU Graz.
[19] Bazant, S. and Oh, B.-H., 'Crack band theory for fracture of concrete', *Materials and Structures.* **16** (1983) 155-177.
[20] Hadl, P. and Tue, N.-V., 'A numerical model to determine the characteristic length of UHPFRC bending beams', in 'Proceedings of UHPFRC 2017', Montpellier, October 2017.
[21] DAfStb, 'Richtlinie Stahlfaserbeton', (Beuth Verag, 2010).
[22] Hadl, P., Kim, H., Tue, N.-V., 'Experimental Investigations on the Scattering in the post cracking tensile behavior of UHPFRC', in 'Proceedings of HiperMat 2016', Kassel, March 2016.